Warm dense matter in extremely small volume - Hydrodynamics of nanofilms triggered by laser irradiation at diffraction limit

N. A. Inogamov, V. V. Zhakhovsky, and V. A. Khokhlov

Citation: AIP Conference Proceedings **1979**, 190002 (2018); doi: 10.1063/1.5045044
View online: https://doi.org/10.1063/1.5045044
View Table of Contents: http://aip.scitation.org/toc/apc/1979/1
Published by the American Institute of Physics

Warm Dense Matter in Extremely Small Volume - Hydrodynamics of Nanofilms Triggered by Laser Irradiation at Diffraction Limit

N.A. Inogamov[1,a)], V.V. Zhakhovsky[2] and V.A. Khokhlov[1]

[1]*Landau Institute for Theoretical Physics, Russian Academy of Sciences, Chernogolovka, Russia*
[2]*Dukhov Research Institute of Automatics (VNIIA), Moscow, Russia*

[a)]Corresponding author: nailinogamov@gmail.com

Abstract. Modern laser techniques combine sophisticated manipulations of a photon bunch with the refined target design. The photon bunch of a femtosecond (fs) laser pulse (duration ~ 100 fs) is just tens microns long (along a laser ray) and one micron thick (in direction transverse to the ray) when it is focused in the diffraction limited regime onto a target. Here the considered targets are films of different thicknesses (from tens nanometers, nm, to 100s nm). Also we compare pulse durations from 0.1 ps to tens of ps. In case of ultrashort laser action there is (i) an ultrafast isochoric transfer of initially solid metal into warm dense matter (WDM) state and (ii) after that molten metal returns back (more slowly) to a crystal (re-solidification finalizes processes initiated at any pulse duration). To study the evolution of these targets under such illumination conditions, a simulation package including two-temperature (2T) (2T - because immediately during and for some time after a fs pulse the electrons are much hotter than the lattice - thus two temperatures different for electrons and ions appear) 1D hydrodynamics code (2T-HD code) and 3D molecular dynamics (MD) code combined with Monte Carlo (MC) method (MD-MC code) are utilized. MC method allows us to take into account significant thermal conductivity of metal, which is important for cooling and re-crystallization of molten matter. The observed processes, including absorption, melting, capillary dynamics of hot liquid and its freezing into solitary nanostructure, produced by such laser electromagnetic fields, are discussed.

INTRODUCTION

Motivations for developing the tightly focusing laser technologies together with impressive list of applications (from plasmonics to medicine and so on) may be found in many papers, e.g., [1–3]. Our analysis [4, 5] shows that the physical picture is based on transfer of solid film into liquid phase, dynamics of kick-off of a film, competition between inertia and capillarity, and fast re-crystallization of molten metal. Re-crystallization is fast in the sense that it overruns the hydrodynamic reforming (hydrodynamic shape changing). Therefore the deformed shape is solidified in its deformed state. This is surprising. Indeed, in our ordinary (~ 1 cm, ~ 1 s) spatiotemporal scales this is like stopping (instantaneous freezing, glaciation) of water flying in fountain; usually in metallurgy we need a supporting mould for casting. Of course, such process (combination of capillary motion with jets, droplets from one side and "instantaneous" solidification from the other side) produces quaint and ornamental structures, see examples in [3, 6–10].

Capillarity plays a leading role specifically in evolution produced by the tight focusing, where a lateral (along illuminated surface) scale of a laser beam is small [4, 5] (because a capillary scale is small). The smallest illuminated spots are of the order of electromagnetic wavelength λ; $\lambda \sim 1$ μm for visible light. Of course, surface tension is also important in the case of large illuminated spots (10s, 100s microns and more in diameter) [11]-[17]. In this case the combined action of inertia, capillarity, and freezing produces chaotic surface structures (CSS) [11]-[17] used as functional surfaces in many applications. CSSs present traces of a long, intensive thermo-mechanical "life" excited by laser [12]: this "life" is composed from capillary foaming, decay of foam (rupture of membranes and threads by their stretching [13]), and fast freezing of remnants of this decay stage. Foam is a liquid-vapor mixture with small volume liquid content. It is interesting that foam topologically is similar to the Voronoi grid of cells (Voronoi polyhedra) studied in past by many great scientists [18]. Foam topology is also similar to the large scale structure of Universe

Shock Compression of Condensed Matter - 2017
AIP Conf. Proc. 1979, 190002-1–190002-6; https://doi.org/10.1063/1.5045044
Published by AIP Publishing. 978-0-7354-1693-2/$30.00

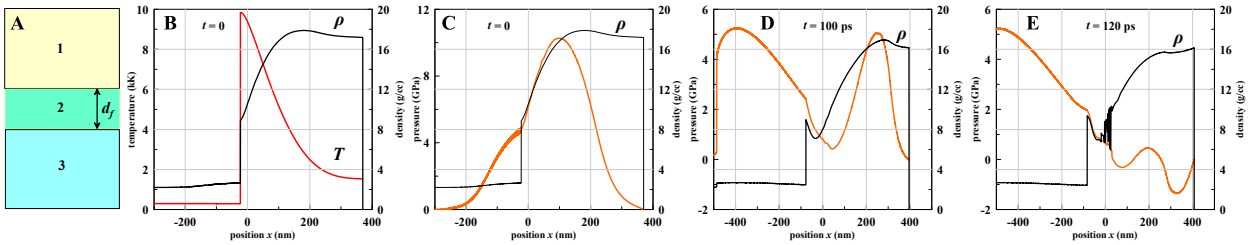

FIGURE 1. A. Geometry of a target, film is in the middle. **B, C.** Density, temperature and pressure profiles at the maximum of intensity $I \propto \exp(-t^2/\tau_L^2)$ of the laser pulse. Half of total absorbed energy is absorbed to the time $t = 0$. Pulse is long therefore the profiles are spatially smooth. Initially the contact between gold at the right side and silica at the left side is in the point $x = 0$. Contact moves to the left side under pressure acting from the hot gold. Motion of the contact increases pressure in silica. Compression wave in gold moves to the vacuum boundary on the right side. Acoustic impedance of silica is small relative to gold, therefore pressures in silica are smaller. We see that near the contact at the time $t = 0$ the gold is in a state significantly above a critical point $\rho_{cr} \approx 5.3$ g/cc, $T \approx 7.8$ kK, $p_{cr} \approx 0.53$ GPa. Initially the film was molten at temperature $T = 1.5$ kK. HAZ covers (at FWHM) approximately one third part of the film. **D.** Expansion of HAZ results in drop of pressure in HAZ at $t = 100$ ps. Compression wave in the gold reflects from the vacuum boundary. Reflection decreases pressure. Therefore pressure in gold is lower relative to silica where a compression wave is near the boundary of silica with vacuum; initial thickness of silica in simulation is 500 nm. This thickness is enough for our purposes (to see fragmentation of gold film) because the gold near surface transfers into fragmented state before the instant when a reflected wave in silica returns to the contact with gold. Thus relatively slow motions in silica cannot affect gold outside the contact. **E.** $t = 120$ ps. Pressure in hot gold near the contact equals to saturated vapor pressure $p_{sat}(T)$. While at slightly larger distance pressure becomes negative because temperature T here is lower and gold keeps partly its resistance against stretching. This causes spallation which manifests itself as sharp fluctuations of density.

with cosmic web from voids, walls, filaments, and nodes [19]; see also "Millennium Simulation - MPA" by V. Springel. CSS is a frozen stamp of this topology on the surface. The CSS (large fluences, few shots) and LIPSS (laser induced periodic surface structures created by interference of incident EM wave with surface plasmon-polaritons) (lower fluences, more shots) are the limiting classes of surface structures, see Fig. 11 in [14]. The bridge between them is still weakly explored. As we will see below, the thermo-mechanical "life" of small spots is also very interesting.

MICRON SIZE ILLUMINATION SPOTS. THICK FILMS, LONG PULSES

Film thickness d_f, duration of laser pulse τ_L, and diameter of a spot, $2R_L$, are important parameters. Thin films and bulk targets have differences and similarities in behavior, as is discussed below. Separation between laser induced motions in thin and bulk targets depends on the listed three parameters and amount of absorbed energy F_{abs}. The larger value F_{abs}, the deeper penetration of motion, and the larger influence on the motion produced by more distant rear-side boundary. Nevertheless, typically a penetration depth is less than diameter ~ 1 μm, thus at the early stages the motion is approximately quasi-one-dimensional (1D) in the sense that the lateral gradients are much less (soft gradients) than the normal ones directed along the direction of laser action. We are interested in situations when action is strong enough to produce ruptures in rarefaction wave and/or inertial expansion and flying-off. The normal gradients are large but only at initial stages, after that they decay to small values. While lateral gradients are connected with fluence distribution along a surface. They are kept at moderate level for a long times, and define transition from quasi-1D to 3D expansion.

This gradual transition from the short-time quasi-1D stage to the long-time 3D motion was studied in [1, 4, 5, 20]. This was the simplest case with a thin film supported by a substrate; thin means that film thickness d_f is less than thickness of a heat affected zone (HAZ) d_T; $d_T \approx 150$ nm for gold and ultrashort pulse. Analysis [1, 4, 5, 20] allows us to understand and describe processes of formation of solitary structures depending on value F_{abs} from cupola like to cone like shapes as F_{abs} increases and at further increase of F to the shape with cone with a jet in the tip and at last to the through hole with complicated rim around at the largest F_{abs}. Dynamics of a supported film was studied in [21]. Interesting effect in nano-crystallization was found. But the approach and resources don't allow to obtain jets and separated droplets in these simulations. A situation with thick films is much more unclear [8] relative to thin films driven by ultrashort pulse. Even quasi-1D flow is less trivial. Predictions about the 3D stage and final shape may be made from the quasi-1D picture. At the present stage of studies we don't have description of 3D flow for thick films.

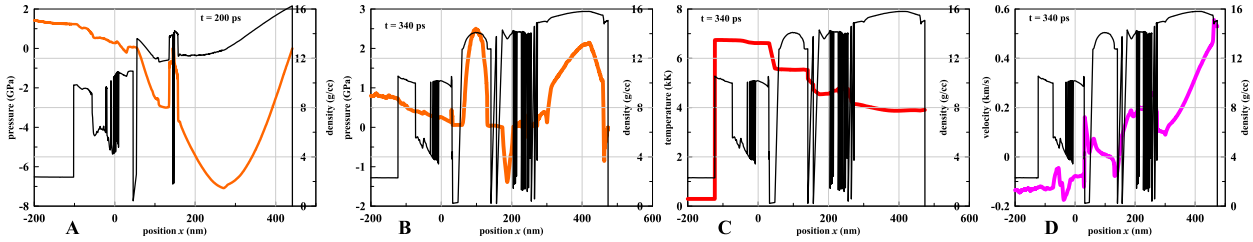

FIGURE 2. A. $t = 200$ ps. Stretching still continues, this cause additional spallations, now away from HAZ. Every spallation causes sharp drop of density. Spallation unloads tensile stress and thus produces spall shocks propagating slightly above speed of sound to the left and right sides from the spall place. This is clearly seen in the point ≈ 140 nm. **B.** $t = 340$ ps. Additional and the last spallation events take place to the right from the point 140 nm. They locates around the point 250 nm at the instant shown. In Fig. 2A we see rather deep well of negative pressures. The left side of this well is hotter. Therefore the last ensemble of spallations take place at the left side of a pressure well. After that pressure decreases to low values; fluctuations of p are caused by oscillations of spall shocks. Therefore further expansion continues in inertial regime. **C.** Fluctuating zones are filled by foam. Heat conduction through foam is suppressed, while inside the continuous intervals conduction works. This causes formation of steps on a temperature profile. **D.** Velocity field at $t = 340$ ps. Internal continuous layers has small velocities, moderate temperature, and significant thickness. They can expand forming cupola like or cupola and jet like solitary structures.

Therefore we have performed 1D 2T-HD simulations shown below, because they shed light onto final 3D effects.

Geometry of 1D simulation is presented in Fig. 1A. Metal film "2" is placed between transparent semispaces "1" and "3". The semispaces may be filled by: vacuum, liquid or solid media. Here we consider the case with vacuum in semispace 1 and silica in semispace 3. A laser pulse may come from the upper or bottom directions. Here a pulse coming from the bottom passes the transparent glass. The film is made from gold, and has thickness $d_f = 370$ nm. This thickness overcomes thickness of HAZ. The pulse duration of 50 ps is relatively long. Therefore the two-temperature (2T) effects are weak and thickness of HAZ is moderate; 2T heat conduction κ is enhanced relative to one-temperature κ; $d_T \approx 150$ nm for ultrashort pulse, while for our pulse $d_T \approx 2\sqrt{\chi\,\tau_L} = 140$ nm for $\chi \sim 1\,\mathrm{cm}^2/\mathrm{s}$, $\tau_L = 50$ ps; in spite of much longer pulse relative to ultrashort case the thickness d_T is of the same order.

Fig. 1B-E shows evolution of a target during and after laser pulse. Absorbed energy is 338 mJ/cm^2. This is large amount of energy. Ablation threshold for bulk gold (Au) in vacuum under the action of ultrashort pulse is $F_{abs}|_{abl} \approx 100\,\mathrm{mJ/cm}^2$ [22–24]. Such pulse heats Au to 2-2.5 kK. In our case F_{abs} is ≈ 3.4 times higher while thickness of HAZ is approximately the same. Therefore temperatures in HAZ are high, see Fig. 1B with a temperature profile.

Highly pressurized hot HAZ expands in both sides decreasing density in HAZ and producing compression waves in Au and silica, see Fig. 1C and 1D. Inertial expansion of Au decreases pressure in HAZ. Contact deceleration of expanding gold by silica increases density of Au near the contact. Hot Au near the contact transits through a binodal curve into two-phase vapor-liquid state in Fig. 1D. Shortly after the instant $t = 100$ ps shown in Fig. 1D the spallation takes place at the right side of the HAZ in Fig. 1E.

Further evolution of a film irradiated by strong and rather long pulse is shown in Fig. 2. We see (i) development of fragmentation to the few rather thick spallation layers, (ii) finishing of fragmentation, and (iii) transfer to a regime of inertial flight. There are three layers moving toward vacuum. The first one has center of mass velocity ≈ 300 m/s, temperature 4 kK, and thickness 200 nm. The middle layer is: 180 m/s, 4.5 kK, 40 nm. The last one is: 20 m/s, 5.5 kK, 100 nm. They all have a chance to form a cupola like solitary structure.

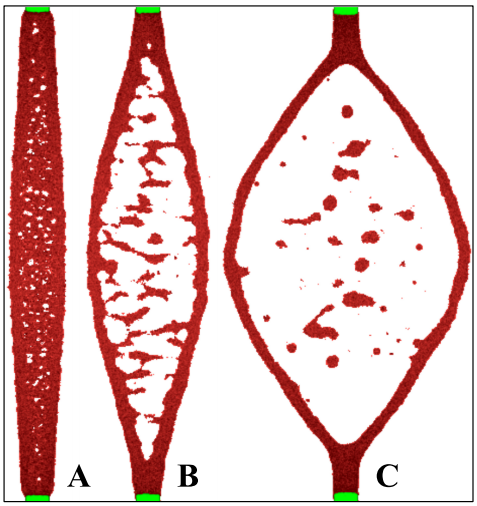

FIGURE 3. Initial stage of decay of heated central region into two halves, $t = 11, 43, 108$ ps. Acoustic time scale for our film is $t_s = d_f/c_s \approx 3$ ps, $d_f = 10$ nm, $c_s \approx 3$ km/s. Maps of central symmetry (CS) parameter are given - green is solid, while red is liquid; side view.

The goal of 2T-HD simulation shown above was to understand, is it possible to form cupola like solitary structures as in the case of thin films $d_f < d_T$ and ultrashort pulses $\tau_L = 0.1-1$ ps in the very different case with thick films and multi picosecond

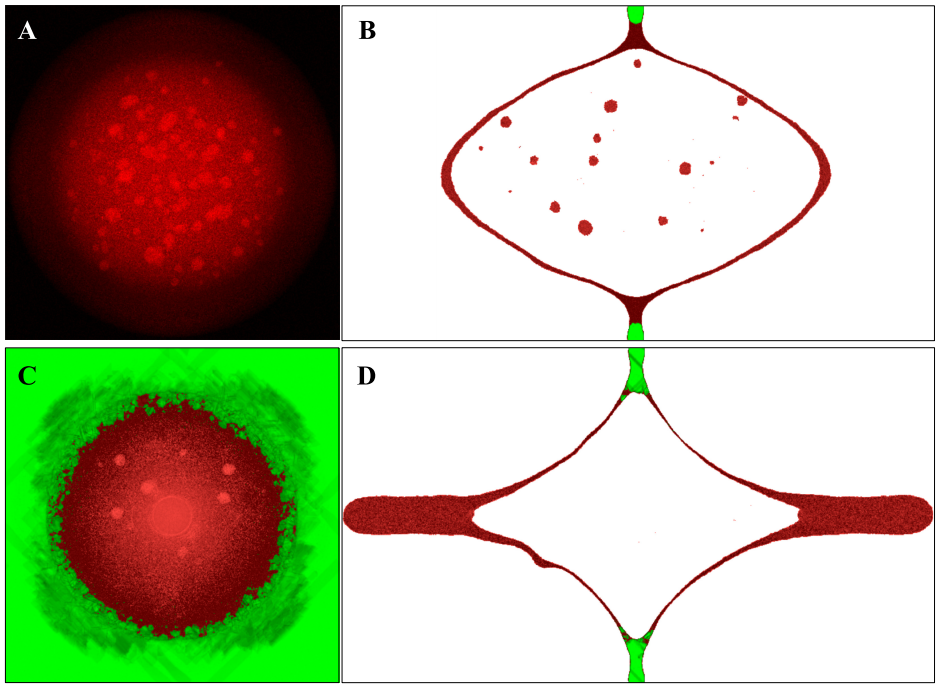

FIGURE 4. Strong deceleration and stopping of flight of the left and right shells by surface tension of liquid gold, $t = 324, 648$ ps; A, C are views from above, while B and D are cross sections. After stopping of the shell the jets begin to grow, which is similar to the case with blistering of a film from substrate [1, 4, 5, 20]. Distributions of central symmetry parameter (CS) are presented. At the stage shown foam decays from the Voronoi polyhedra like structure into droplets created from the nodes of structure. Droplets fly faster than decelerating shell because they move freely. This causes impacts of droplets onto shell. Flying droplets are hotter than the shell, therefore they are clearly seen on the maps A and C. Number of droplets decreases with time as seen from A and C. B and D are cross sections, therefore none of droplets come into this cross-section at the time shown in C and D, thus D is empty.

pulses. Results show that this is possible. In the next Section we will demonstrate that collection of remnants of decay of foam onto surface of the spallation layer (or shell) doesn't break off the spallation layer; foam exists in the gaps between layers. Also it seems that cupola will survive after collision of two spallation layers with each other.

THIN FREESTANDING FILMS, ULTRASHORT PULSES

In previous simulations of nanobumps with jets [1, 4, 5, 20] the case with thin film and ultrashort pulse was considered. In Section 2 we present results for thick film and long pulse. Here we consider another new interesting case - the freestanding film. It differs from the supported case when spallation cupola is empty; here foam fills cavity. The film cover the square 204*204 nm*nm and is 10 nm thick. It contains $23.3 \cdot 10^6$ gold atoms. Film was heated during the first picosecond by Langevin thermostat to $T(r, t = 0) = T_1(1 + \cos^2((\pi/2)(r/R)))$ inside the circle $r < R$, and to T_1 in the region between the sides of the square 204*204 nm*nm and the circle of radius R, where $T_1 = 3$ kK, $R = 100$ nm; the thermostat heats atoms in lateral directions - the normal component of velocity wasn't heated. After that at $t > 1$ ps the thermostat working inside the circle has been switched off. While the thermostat working in the region between square and circle begins permanently support temperature $T_2 = 0.5$ kK. This is a sink of heat coming (thanks to electron heat conduction) from the hot central part of a laser spot; conduction is described by the MC block. The sink acts like the laterally infinitely large film with cold periphery outside the heated circle.

Due to high central temperature (and thus pressure) the film decays into two halves flying in the opposite directions, see Figures 3 and 4B, 4D. Surface tension decelerates this flight and stops it as it is shown in Fig. 4. In our conditions the stopping takes place before freezing of a shell. Therefore jets have possibility to develop, see Fig. 4D.

Late stages are shown in Figures 5 and 6. We see development of long jets, their decay into droplets thanks to Rayleigh-Plateau instability, and final freezing of the remnants of jets, while liquid droplets fly away. Surprising

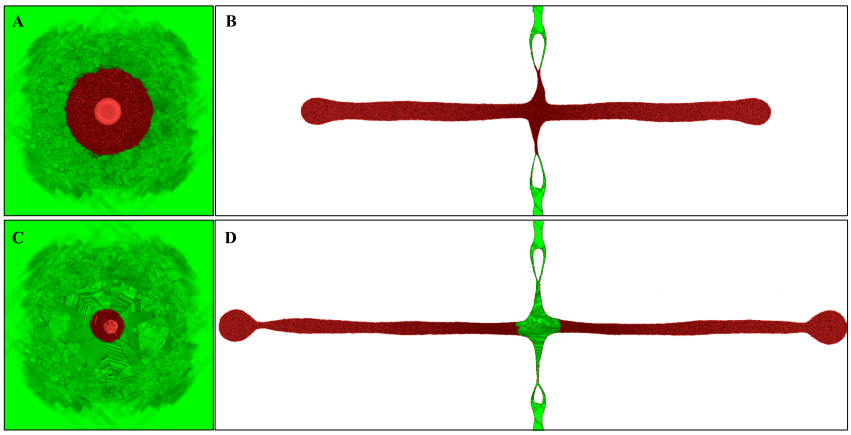

FIGURE 5. t = 1080 ps (A,B); t = 2160 ps (C,D). Jets fly far away, while the shells return back and impact each other. Freezing propagating radially along the film comes closer and closer to the jets. In D beginning of re-crystallization of the base of the jet is shown. Droplets at the ends of the jets are ready to separate due to Rayleigh-Plateau instability. Remarkable crystallin structure forms around the base, see map C. Please, enlarge picture to see details better. A rim from large densely packed lamellar crystallites appear; they impede each other. These crystallites in frame C develop from the small randomly oriented crystallites in frame A.

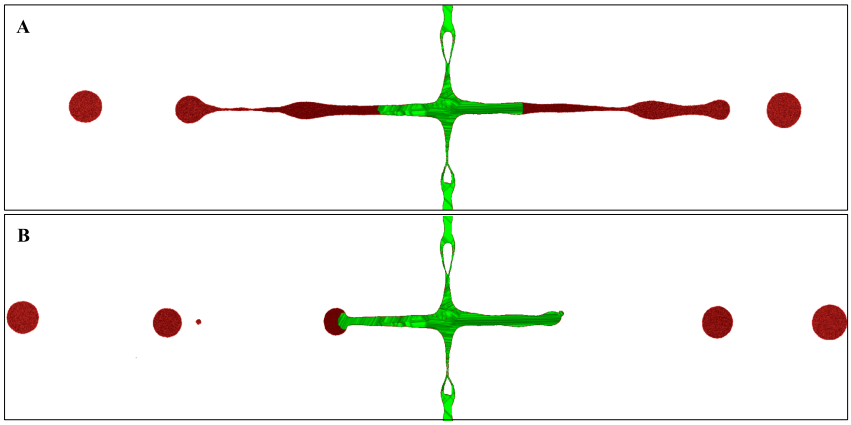

FIGURE 6. Very late stages when the jets crystalize. Before final solidification they send out few liquid droplets. Compare A and B. You see how re-crystallization proceeds along the jets. **A.** t = 3240 ps. **B.** t = 4244 ps. The droplet remains at the left jet.

lamellar crystallization is seen in Fig. 5C.

DISCUSSION AND CONCLUSION

Above we present two new situations with the thick films and long pulses (Section 2) and jetting of freestanding films (Section 3), which are different from those discussed in [1, 4, 5, 20] where the thin supported films and an ultrashort laser pulses were studied. People have observed such solitary structures experimentally, and say that they correspond to phenomena equal to jetting or splashes when a droplet falls down to water, see Figure 1b,c in [3]. We cannot agree with this. They are similar only in the sense that capillarity plays the significant role. But dynamics of fast laser heating and kick-off of a film from substrate is special and different from that in the case of droplet falling to water. The other difference is in the fact that in our case development is defined by competition between capillarity and freezing: phase transition of the first order cardinally changes mechanical properties and therefore sharply changes motion.

The research has been performed under financial support from Russian Science Foundation (RSCF) (prolonged project No. 14-19-01599).

REFERENCES

[1] A. Kuchmizhak, O. Vitrik, Yu. Kulchin, D. Storozhenko, A. Mayor, A. Mirochnik, S. Makarov, V. Milichko, S. Kudryashov, V. Zhakhovsky and N. Inogamov, Nanoscale **8,** pp. 12352-12361 (2016)

[2] U. Zywietz, A. B. Evlyukhin, C. Reinhardt, and B.N. Chichkov, Nature Communications **5,** p. 3402 (2014)

[3] Y. Nakata, N. Miyanaga, K. Momoo, and T. Hiromoto, Japanese J. Appl. Phys. **53,** 096701 (2014)

[4] N.A. Inogamov, V.V. Zhakhovskii, and V.A. Kholhlov, J. Experim. Theor. Phys. (JETP) **120,** No. 1, pp. 15-48 (2015)

[5] N.A. Inogamov, V.V. Zhakhovsky, V.A. Khokhlov, Yu.V. Petrov, and K.P. Migdal, Nanoscale Res. Lett. **11,** 177 (13 pages) (2016)

[6] C. Unger, J. Koch, L. Overmeyer, and B.N. Chichkov, Optics Express **20,** No. 22, pp. 24864-24872 (2012)

[7] D.A. Zayarny, A.A. Ionin, S.I. Kudryashov, S.V. Makarov, A.A. Rudenko, S.G. Bezhanov, S.A. Uryupin, A.P. Kanavin, V.I. Emel'yanov, S.V. Alferov, S.N. Khonina, S.V. Karpeev, A.A. Kuchmizhak, O.B. Vitrik, Yu.N. Kulchin, JETP Lett. **101,** No. 6, pp. 394-397 (2015)

[8] P.A. Danilov, D.A. Zayarny, A.A. Ionin, S.I. Kudryashov, T.T.H. Nguyen, A.A. Rudenko, I.N. Saraeva, A.A. Kuchmizhak, O.B. Vitrik, Yu.N. Kulchin, JETP Lett. **103,** No. 8, pp. 549-552 (2016)

[9] D. Wortmann, J. Koch, M. Reininghaus, C. Unger, C. Hulverscheidt, D. Ivanov, and B.N. Chichkov, J. Laser Applications **24,** 042017 (2012)

[10] M. Armstrong, *The evolution of ultrafast compression*, SIMES Seminar, (2015) https://simes.stanford.edu/events/mike-armstrong-simes-seminar

[11] A.Ya. Vorobyev and Chunlei Guo, Optics Express **14,** No. 6, pp. 2164-2169 (2006)

[12] R. Fang, A. Vorobyev, and C. Guo, Light: Sci. Appl. **6,** No. 3, e16256 (2017)

[13] N.A. Inogamov, V.V. Zhakhovsky, S.I. Ashitkov, Yu.N. Emirov, A.Ya. Faenov, T.A. Pikuz, M. Ishino, M. Kando, N. Hasegawa, M. Nishikino, T. Kawachi, M.B. Agranat, A.V. Andriash, S.E. Kuratov, and I.I. Oleynik, J. Phys.: Conf. Ser. **500,** 112070 (2014)

[14] N.A. Inogamov, V.V. Zhakhovsky, S.I. Ashitkov, Yu.N. Emirov, A.Ya. Faenov, Yu.V. Petrov, V.A. Khokhlov, M. Ishino, B.J. Demaske, M. Tanaka, N. Hasegawa, M. Nishikino, S. Tamotsu, T.A. Pikuz, I.Y. Skobelev, T. Ohba, T. Kaihori, Y. Ochi, T. Imazono, Y. Fukuda, M. Kando, Y. Kato, T. Kawachi, S.I. Anisimov, M.B. Agranat, I.I. Oleynik, V.E. Fortov, Engineering Failure Analysis **47,** pp. 328-337 (2015)

[15] E.L. Gurevich, Phys. Rev. E **83,** 031604 (2011)

[16] S.I. Ashitkov, S.A. Romashevskii, P.S. Komarov, A.A. Burmistrov, V.V. Zhakhovskii, N.A. Inogamov, and M.B. Agranat, Quantum Electronics **45,** No. 6, pp. 547-550 (2015)

[17] N.A. Inogamov, V.V. Zhakhovsky, V.A. Khokhlov, S.I. Ashitkov, Yu.N. Emirov, K.V. Khichshenko, A.Ya. Faenov, T.A. Pikuz, M. Ishino, M. Kando, N. Hasegawa, M. Nishikino, P.S. Komarov, B.J. Demaske, M.B. Agranat, S.I. Anisimov, T. Kawachi, and I.I. Oleynik, J. Phys.: Conf. Ser. **510,** 012041 (2014)

[18] https://en.wikipedia.org/wiki/Voronoi-diagram

[19] https://en.wikipedia.org/wiki/Observable-universe#Large-scale-structure

[20] P.A. Danilov, D.A. Zayarny, A.A. Ionin, S.I. Kudryashov, A.A. Rudenko, A.A. Kuchmizhak, O.B. Vitrik, Yu.N. Kulchin, V.V. Zhakhovsky, N.A. Inogamov, JETP Lett. **104,** No. 11, pp. 759-765 (2016)

[21] D.S. Ivanov, Zh. Lin, B. Rethfeld, G.M. O'Connor, T.J. Glynn, and L.V. Zhigilei, J. Appl. Phys. **107,** 013519 (2010)

[22] N.A. Inogamov, V.V. Zhakhovskii, S.I. Ashitkov, Yu.V. Petrov, M.B. Agranat, S.I. Anisimov, K. Nishihara, V.E. Fortov, J. Experim. Theor. Phys. (JETP) **107,** No. 1, pp. 1-19 (2008)

[23] B.J. Demaske, V.V. Zhakhovsky, N.A. Inogamov, I.I. Oleynik, Phys. Rev. B **82,** 064113 (2010)

[24] G.E. Norman, S.V. Starikov, and V.V. Stegailov, J. Experim. Theor. Phys. (JETP) **114,** No. 5, pp. 792-800 (2012)